Macromolecular Research, Vol. 14, No. 1, pp 45-51 (2006)

# Competition between Phase Separation and Crystallization in a PCL/PEG Polymer Blend Captured by Synchronized SAXS, WAXS, and DSC

**Wei-Tsung Chuang, U-Ser Jeng*, and Hwo-Shuenn Sheu**

*National Synchrotron Radiation Research Center101 Hsin-Ann Road, Hsinchu Science Park Hsinchu 30076, Taiwan*

**Po-Da Hong**

*Department of Polymer Engineering, National Taiwan University of Science and Technology, Taipei 10673, Taiwan*

*Received September 22, 2005; Revised November 30, 2005*

**Abstract:** We conducted simultaneous, small-angle, X-ray scattering/differential scanning calorimetry (SAXS/DSC) and simultaneous, wide-angle, X-ray scattering (WAXS)/DSC measurements for a polymer blend of poly(ε-caprolactone)/poly(ethylene glycol) (PCL/PEG). The time-dependent SAXS/DSC and WAXS/DSC results, measured while the system was quenched below the melting temperature of PCL from a melting state, revealed the competitive behavior between liquid-liquid phase separation and crystallization in the polymer blend. The time-dependent structural evolution extracted from the SAXS/WAXS/DSC results can be characterized by the following four stages in the PCL crystallization process: the induction (I), nucleation (II), growth (III), and late (IV) stages. The influence of the liquid-liquid phase separation on the crystallization of PCL was also observed by phase-contrast microscope and polarized microscope with 1/4λ compensator.

*Keywords*: phase separation, crystallization, polymer blend, poly(ε-caprolactone), poly(ethylene glycol).

## Introduction

X-ray scattering often provides critical structural information in understanding the mechanisms of phase transformation. Especially, in time-resolved experiments a synchrotron radiation (SR) X-ray source, characterized by tremendously high photon flux and wide energy band, is usually indispensable. With the advances of X-ray sources and experimental techniques, SR X-ray scattering nowadays is often combined with other measurements such as DSC,[1-5] light scattering,[6] dielectric spectroscopy,[7] Raman spectra,[8] and infrared spectroscopy.[9] The integrated study for the structural characteristics, the thermal, electrical, and other physical properties of a sample system offers many advantages over individual experiment, particularly, in correlating structure characteristics with properties or in resolving or identifying a mechanism of, for instance, crystallization-related phase separation in polymer blends.

Based on simultaneous SAXS and WAXS measurements, Terrill *et al.*[10] suggested that long-range density fluctuations occurred prior to the development of crystalline peaks during the crystallization of isotactic polypropylene, when the density fluctuations developed via spinodal decomposition. In another case, Balta-Calleja *et al.*[11] found that an ordering process preceded the cold crystallization in their system by simultaneous SAXS, WAXS, and dielectric spectroscopy. Tashiro *et al.*,[12] inspired by the result of simultaneously measured WAXS and Raman spectra, also proposed a relationship between the stretching of polymer chains and the crystallization behavior observed.

Classically, the complex mechanism of polymer crystallization is understood on the basis of nucleation-followed-by-growth. Nevertheless, the recently observed behavior for the early stage of polymeric crystallization challenges this classical view.[10-14] The precursory change in structure during the induction period prior to crystallization has been studied by several groups using various scattering techniques. For instance, in a cold crystallization, Imai *et al.*[13] monitored the growth of a small SAXS peak during the induction period of crystallization in their polymer system. And the observed growth behavior could be explained by the spinodal mechanism of Chan-Hilliard theory (Note, the peak monitored was attributed to the increase of parallel ordering of polymer segments, instead of the formation of lamellar structure.). Furthermore, the mechanisms of liquid-liquid phase separation (LLPS) and early stage crystallization in polymer blends have also been individually and extensively investigated.[15-18] However, the dynamics relating to the competition between

*Corresponding Author. E-mail: usjeng@nsrrc.org.tw

crystallization and LLPS in semicrystalline/amorphous polymer blends is relatively less studied due to the complicated coupling between LLPS and crystallization.

When temperature quenched below the melting temperature of the crystalline polymer of a polymer blend, simultaneous LLPS and crystallization can be expected. Thermodynamically, LLPS occurs prior to crystallization.[19] Nevertheless, the kinetic competing law is *the fastest wins*. The occurring sequence of LLPS and crystallization cannot determine alone the final morphology; the competition between these two processes also matters. And when LLPS couples with crystallization, a polymer blend can be kinetically trapped in a non-equilibrium state, leading to a structure or morphology that may influence strongly the properties of the blend. Thus, it is possible to tailor the final morphology of a polymer blend for specific applications via a kinetic control of the process of LLPS and crystallization. In a previous paper,[20] we have discussed in detail the phase separation kinetics of a polymer blend poly($\varepsilon$-caprolactone)/poly(ethylene glycol) (PCL/PEG) by small angle light scattering. In this study, using simultaneous SAXS/DSC and WAXS/DSC we focus on the crystallization kinetics of the PCL/PEG blend, under the influence of an ongoing phase separation.

## Experimental

**Material.** PCL and PEG were received from Aldrich Chem. Co., with weight-average molecular weights ($M_w$) of 10,000 and 400 Da, respectively. The two components were molten-mixed for a PCL/PEG blend, with a weight ratio of 7:3.

**Measurement.** Simultaneous SAXS/DSC and WAXS/DSC were performed at beamlines BL01B (a SAXS setup) and BL01C (powder X-ray scattering endstation) of the National Synchrotron Radiation Research Center (NSRRC). In the SAXS/DSC measurement, the incident beam, extracted from a superconducting-wavelength-shifter (SWLS) X-ray source, was focused by a toroidal mirror and monochromated to 10.5 keV (wavelength $\lambda$ = 1.181 Å) using a Ge (111) double-crystal monochromator. The 0.5 mm diameter beam used was mainly collimated by one set of slits and two sets of Ta pinholes, arranged in ~ 5 m. The sample was sealed inside a DSC cell of Mettler Toletro (FP90). The SR beam intensity was high enough to afford the ~50% intensity loss due to the absorption of the two thin glass windows (each of 100 $\mu$m) of the DSC cell. With a sample-to-detector distance of 1571.4 mm and a beam stop of 4 mm diameter, we collected SAXS data using a 50 mm linear detector of 80 $\mu$m pixel resolution. All the SAXS data were corrected for sample transmission, background, and the detector sensitivity. And the wavevector transfer $q(=4\pi\sin(\theta/2)/\lambda)$, defined by the scattering angle $\theta$ and the wavelength $\lambda$ of the X-rays, was calibrated by a standard sample of silver behenate. The detailed SAXS setup and instrument calibration were reported previously.[21]

In WAXS/DSC measurement, the incident beam from the same SWLS X-ray source was focused by a toroidal mirror, and monochromated to 20 keV (wavelength $\lambda$ = 0.620 Å) by a Ge (111) double-crystal monochromator. The beam was mainly collimated by a 20 cm collimator of 1 mm dia. channel. And the sample was sealed in the DSC cell as that used in the SAXS/DSC measurement. The high energy photons used here could penetrate easily the two thin glass windows sealing the DSC cell, with little loss of the beam intensity. WAXS data were collected using imaging plates (IP, of an area = 20 × 40 cm$^2$ and a pixel resolution of 100 $\mu$m) curved with a radius equivalent to the sample-to-image plate distance (280 mm). With two square panels for confining the exposure area within a strip of 0.3 × 40 cm$^2$, the IP plate took sequentially ~36 exposures for the time-dependent WAXS, with 120 s for each exposure. The scattering angle $\theta$ was calibrated by a mixture of silver behenate and silicon powders.

Morphology transitions during the crystallization and phase separation of the polymer blend were observed on a hot-stage (Linkam THMS-600), using the polarizing microscope (Leica DMLP) and photomicrographs. Crystalline domains were observed with an additional $\lambda/4$ compensator, whereas the phase-contrast mode was used for observing LLPS.

**Lamellar Model for SAXS Data Analysis.** Polymers of a crystalline-amorphous lamellar structure can be characterized using one-dimensional correlation function $\gamma(x)$ Fourier-transformed from the corresponding one-dimensional SAXS data $I(q)$ measured,[22] namely,

$$\gamma(x) = \frac{1}{Q}\int_0^\infty I(q)q^2\cos(qx)dq \tag{1}$$

where the scattering invariant $Q$ can be expressed as

$$Q = \int_0^\infty I(q)q^2dq \tag{2}$$

Since SAXS data are usually collected in a limited angular range, it is necessary to extrapolate data in both high-$q$ and low-$q$ regions before the Fourier transformation. The high-$q$ data can be extrapolated using the Porod-Ruland model,[23]

$$I(q) = K_p\frac{\exp(-\sigma^2q^2)}{q^4} + I_b \tag{3}$$

where $K_p$ is the Porod constant and $I_b$ the background intensity arising from thermal density fluctuations. The parameter $\sigma$ relates to the thickness between the crystalline and amorphous phases. On the other hand, the extrapolation for the zero-$q$ behavior can be done by fitting the SAXS data in the low-$q$ region with the Debye-Bueche model,[24,25]

$$I(q) = \frac{I(0)}{(1+q^2\xi^2)^2} \quad (4)$$

with the correlation length $\xi$. Once $K_p$, $I_b$, $\sigma$, and $\xi$ are ready, $\gamma(x)$ can be deduced.

## Results and Discussion

**Imaging Result.** In Figure 1, the binodal, spinodal, and melting curves are shown in the equilibrium phase diagram of the PCL/PEG blend. The binodal curve is drawn from the data for cloud-point measured, whereas the spinodal curve is determined based on the linear Cahn-Hilliard theory as described in our previous report.[20] As shown in Figure 1, the PCL/PEG blend has an upper-critical-solution-temperature (UCST) type of phase diagram. The nucleation-and-growth (NG) and the spinodal decomposition (SD) take place, respectively, in the metastable region between the binodal and spinodal curves and in the unstable region below the spinodal curve. In a crystalline/amorphous polymer blend, the phase separation and crystallization coexist and compete in the region below the melting curve. And the competition between the LLPS and crystallization, relating to the kinetic trapped morphology, can be complicated and very much cooling-history dependent.

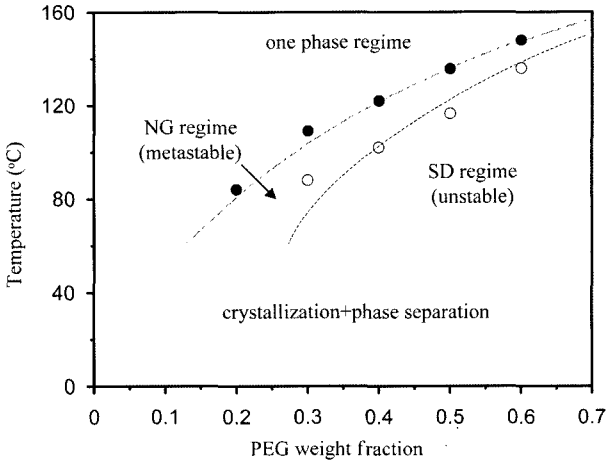


**Figure 1.** Phase diagram of the PCL/PEG blend. The filled circles are obtained from light scattering measurements for PCL/PEG blends with various compositions. The solid, dotted, and dash-dotted curves are eye-guiding lines drawn for the binodal curve, the spinodal curve, and the melting line, respectively.

When temperature quenched to an isothermal crystallization temperature of $T_c$=48 °C, below the melting temperature of PCL (62 °C), the morphology observed for the PCL/PEG blend in the beginning (Figure 2(a)) illustrates a LLPS without crystallization. This result is thermodynamically favored

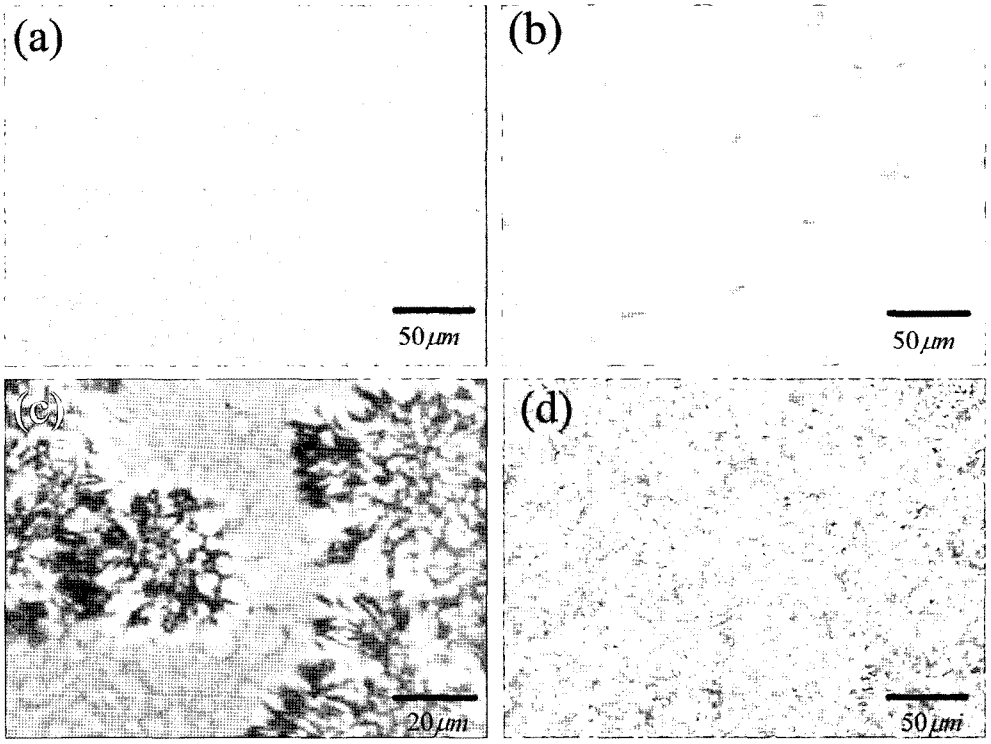


**Figure 2.** The time-dependent morphology evolution of the PCL/PEG blend quenched from a melting state to an isothermal crystallization temperature 48 °C. The images were observed at $t$=60 sec (a), 2,520 sec (b), 4,060 sec (c), and 5,200 sec (d), by a phase-contrast optical microscope for (a) and a polarizing microscope with $\lambda/4$ compensator for (b), (c), and (d).

due to the fact that PCL supercooled below the melting temperature is short of free energy for crossing over the energy barrier of the formation of stable nuclei. Thus, the spontaneous spinodal decomposition usually precedes the polymeric crystallization. For this reason, the liquid-liquid phase boundary can still affect the crystalline morphology during a kinetic process, despite the final crystal-liquid equilibrium structure below the melting temperature is eventually determined by thermodynamics. While the phase separation proceeds continuously as a background environment, PCL starts the nucleation process, as captured in Figure 2(b). Then, the PCL nuclides develop into PCL-rich domains which finally aggregate into the early stage's spherulites, of a sheaf-like morphology. In the meanwhile, no PCL crystal can be observed in the PEG-rich domains because of too little PCL in the PEG-rich domains for nucleation. As time goes on, the sheaf-like domains of PCL continue to grow and repel the PEG-rich domains. Finally, in Figure 2(d), the PCL spherulite domains sweep over the whole phase-separated system, including the PEG rich domains. From Figure 2, the characteristic size of LLPS is obviously smaller than that of the PCL spherulites in the PCL/PEG blend of a weight ratio of 7/3. As we have observed in Figure 2(c), small PEG domains are expelled outside of spherulites and piled up along the borders of the growing spherulites, due likely to the high mobility of the PEG (of a low molecular weight). In Figure 2(d), the segregated, interfibrillar or interspherulitic[26,27] PEG domains characterize the late stage of crystallization.

Below, using the X-ray scattering results, we discuss the development of crystalline structure and nano-to-meso scales density fluctuations in the system.

**Scattering Result.** Figure 3 shows the time-resolved SAXS/DSC and WAXS/DSC profiles obtained during the isothermal crystallization of the PCL/PEG blend, when the sample temperature jumped from 160 (one phase) to 48 °C below the melting temperature (62 °C) of PCL. This designated high isothermal crystallization temperature $T_c$ results in a slow crystallization rate of PCL, and allows a detailed examination on the structural evolution using the time-dependent of SAXS/DSC and WAXD/DSC, of a moderate time resolution of a few minutes.

In the time-dependent SAXS profiles shown in Figure 3(a), a detectable broad halo centering in the vicinity of $q$=0.031 Å$^{-1}$ first appears at $t$~2,000 s. The broad halo grows gradually and develops into a relatively sharp peak at $t$~ 4500 s. As mentioned previously, the appearance of a scattering peak usually signifies the formation of well defined lamellar stacks in typical crystallizable polymers. As the crystallization proceeds (see below), the scattering peak shifts gradually to a larger $q$~0.038 Å$^{-1}$, indicating a condensing of the lamellar spacing, specifically, the long period of lamellar stacks.

We use the density correlation function $\gamma(x)$ extracted from the SAXS data to quantitatively describe the structural evolution of the system. A typical example shown in the inset of Figure 3(a) illustrates the correlation function obtained from the SAXS data measured after the LLPS and crystallization complete ($t$~4,100 s). The first maximum of $\gamma(x)$ corresponds to the long period $L$ of the lamellae. The thickness of the thinner phase of the lamellar stacks $l_1$ can be estimated from the position of the first minimum of the correlation function,[22] whereas the thickness of the thicker phase of the lamellar stacks can be deduced from $l_2=L-l_1$. At the late stage of crystallization, the value of $L$ determined by the first maximum of $\gamma(x)$ is 15.4 nm, with $l_1$=7.1 nm and $l_2$=8.3 nm. The three structural parameters together sug-

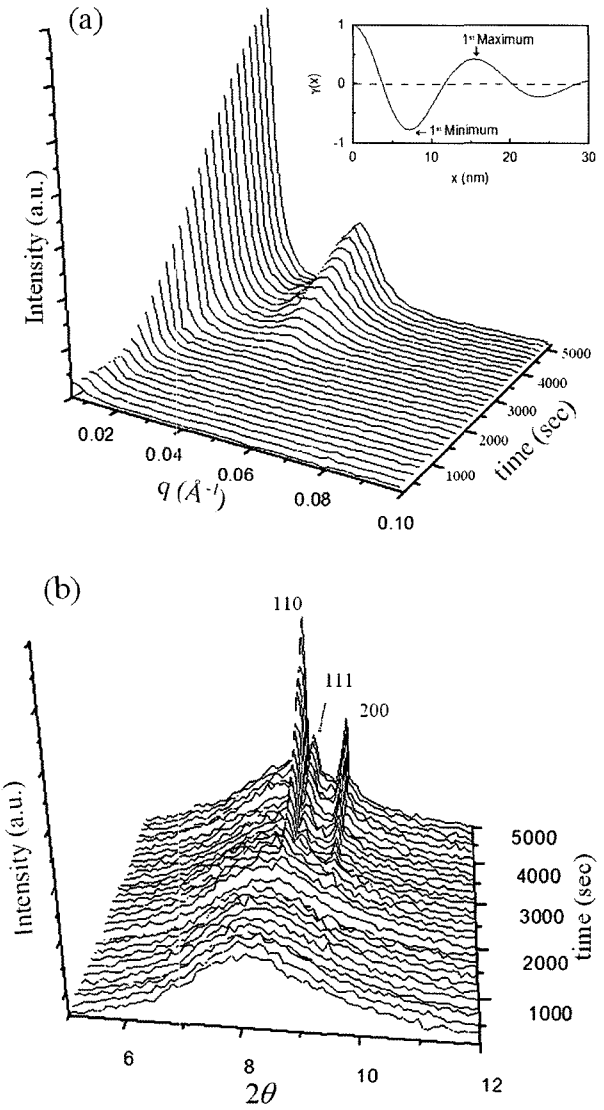


**Figure 3.** Time-dependent SAXS (a) and WAXS (b) profiles observed during the same isothermal crystallization of the PCL/PEG blend at 48 °C. The inset of (a) is a typical one-dimensional correlation function extracted from the SAXS data measured at $t$ ~4,100 s.

gests that the linear fraction of crystallinity is either 0.46 ($X_1=l_1/L$) or 0.54 ($X_2= l_2/L$). In our case, the bulk crystallinity $\Phi_c$ determined by DSC is ca. 0.47. To be consistent with the DSC result, we assign $l_1$ to be the thickness of the amorphous layer $l_a$, and $l_2$ the thickness of crystalline layers $l_c$, respectively, due to the consideration that $\Phi_c$ determined from DSC must be substantially smaller than the linear crystallinity obtained from SAXS for a non-ideal lamellar system. The lamellar thickness of PCL ($l_c$~8 nm) extracted is consistent with that (7~8 nm) obtained by Nojima *et al.*.[28] With the same method described above, the evolutions of $L$, $l_c$, $l_a$, and $Q$ values during the process of LLPS and crystallization are extracted from the series of time-dependent SAXS profiles, and the result is summarized in Figure 4.

In Figure 3(b), the time-dependent WAXS profiles for the system measured under the same conditions are synchronized

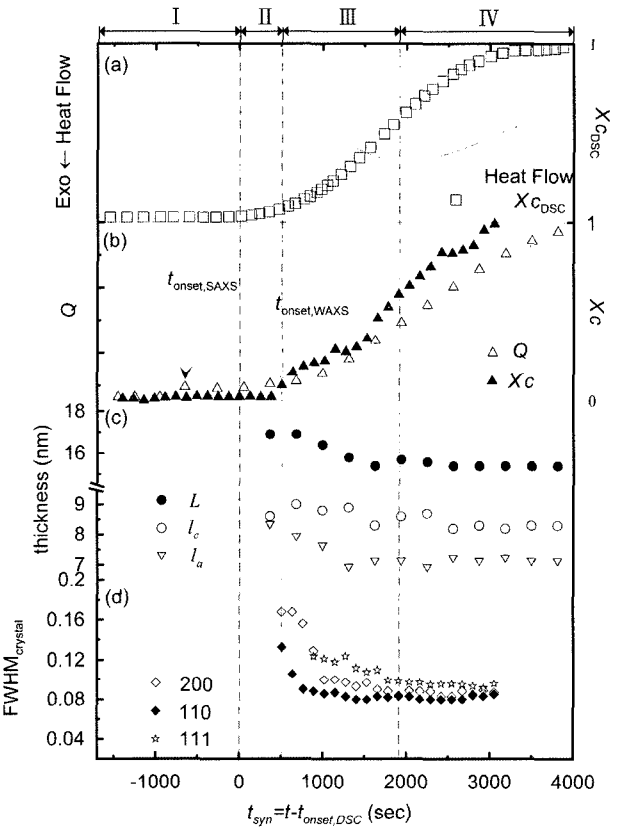


**Figure 4.** The time-dependent evolutions of the exothermic trace and crystallinity $X_{c,DSC}$ (from DSC) (a), scattering invariant $Q$ (from SAXS) and crystallinity $X_c$(from WAXS) (b), and the long period $L$, crystalline thickness $l_c$, and amorphous thickness $l_a$ (from SAXS) (c), and the FWHM of the 110, 111 and 200 crystalline reflections (from SAXS) (d), for the PCL/PEG system in an isothermal crystallization at 48 °C. The arrows in (b) indicate the onset times of the long range density fluctuation ($t_{onset,SAXS}$) and the crystallization ($t_{onset,WAXS}$), respectively. The shaded area across (c) and (d) illustrates the correlation between the crystallization and the formation of lamellar domains.

with that for the SAXS measurement, through the common DSC curves measured. In the beginning, WAXS profiles show only a diffuse halo scattering. Then, three discernible crystalline peaks appear at $t$~2,200 s, and develop gradually with time. The three peaks are assigned to be the crystalline reflections of the planes indexed by 110, 111, and 200 of the orthorhombic unit cell of PCL crystals.[29]

In order to compare SAXS/DSC with WAXS/DSC results, the SAXS and WAXS data are synchronized by the onset time of the exothermic DSC curves, $t_{syn}=t-t_{onset,DSC}$. Using the synchronized time scale $t_{syn}$ shown in Figure 4, we display the structural evolution extracted from the SAXS and WAXS data for the PCL/PEG blend, which can be characterized by four distinct stages: the induction stage (I), the nucleation stage (II), the growth stage (III), and the late stage (IV), according to the kinetics process of the crystallization of PCL.

During the induction stage (I), there is no heat flow before $t_{onset,DSC}$ (or $t_{syn}=0$) (Figure 4(a)), indicating a "crystallization induction period", namely, a characteristic waiting time prior to the nucleation. Figure 4(b) exhibits the time evolution of the invariant $Q$ and the crystallinity $X_c$ extracted from SAXS and WAXS results, respectively. We have estimated the relative degree of crystallinity, $X_c$, basing on the assumption that the integrated 110-reflection peak intensity is directly proportional to $X_c$. Interestingly, both $Q$ and $X_c$ follow a typical exponential growth curve. In Figure 4(b), the two arrows denote, respectively, the onset times when $Q$ and $X_c$ deviate from the baselines. The significant difference between the two onset times may imply that density fluctuations precede the crystallization in the system. The similar time lag of the crystallization has also been detected in other polymeric crystallizations.[5,10,11,30] Furthermore, the starting time of the heat flow in the DSC data marks the beginning of the region II, whereas the time for the frist appearance of the crystalline peaks in WAXS data marks the end of the region II. These two characteristic times are used to define of the region II-the nucleation stage.

On the synchronized time scale, we have a time sequence of $t_{onset,SAXS} < t_{syn} < t_{onset,WAXS}$. These three characteristic times mark, respectively, the first observation of non-trivial values of $Q$, DSC heat flow, and $X_c$, respectively. In addition, the previous result from the polarized microscopy suggests that LLPS of the PCL/PEG blend occurs much earlier than any of these characteristics times. Note, the LLPS could not be observed by the current SAXS measurement due to the limited-$q$ range studied. As a consequence, the large phase-separated domains of a size of ~5 $\mu$m (see Figure 2(a)) in the system contribute little to the $Q$ value shown in Figure 4(b). We, therefore, mainly attribute the non-trivial $Q$ values observed between $t_{onset,SAXS}$ and $t_{syn}$ to the density fluctuations of a nano-to-meso scale in the system. In fact, it is thermodynamically favored to have local density fluctuations beforehand in overcoming the energy barrier of nucleation for the formation of crystallization nuclei.

The nucleation stage (II) between $t_{syn}$=0 and $t_{onset,WAXS}$ is defined for the time zone where the exothermic behavior of the system is observed by DSC (in Figure 4(a)) yet no crystalline peaks can be observed by WAXS (Figure 4(b)). Following the nucleation period is the time zone for the growth stage (III) characterized by the fast changes in the crystalline structure of PCL, starting from $t_{onset,WAXS}$ and finishing before the late stage (IV). In the late stage of crystallization (stage IV), the lamellar domains of PCL (crystallinity) continue to grow in number, with stabilized crystalline structure and domain size. Interestingly, within the time resolution (a minute) of the time-dependent SAXS and WAXS measurements, the lamellar peak in SAXS occurs with the concomitant emergence of the crystalline peaks of PCL in the WAXS, as marked out by the shaded area across Figure 4(c) and (d). The result implies a correlation between the three-dimension packing and the lamellar stacking. Pretransitional density fluctuations prior to the nucleation have already been confirmed in many systems of polymer crystallization,[10-14] including the pretransition SAXS peak observed by Imai *et al.* in the induction period.[13] Although we did not capture the pretransition SAXS peak in our system due to the limited SAXS $q$-range studied, the noticeable increase of the scattering invariant $Q$ detected in the induction stage (I) strongly suggests that a precursory ordering of the polymers chains due to long-range density fluctuations occurs before the crystallization in the PCL/PEG system.

The correlations between the drastic changes in $Q$, $X_c$, $L$, $l_a$, and the crystalline size (inverse proportional to the full-width-half-maximum of the crystalline peaks, $FWHM_{crystal}$) in the growth stage (III) (Figure 4 (b), (c), and (d)), illustrate well the growth characteristics of the PCL domains in the system. In the growth regime, PCL crystalline domains formed concomitantly with the appearance of the lamellar domains since $t_{onset,WAXS}$. And the crystalline domain structure (observed by WAXS) builds mainly along the lamellar plan (200, 110 plans as revealed in Figure 4(d)), while the lamellar domains grow with an increasingly compacted long period (observed by SAXS). The decrease of the long period during the growth of a lamellar structure has been widely observed in semicrystalline polymers. The decrease is generally attributed to a rearrangement of bent lamellae appearing in the beginning of the crystallization[31] or a thinning of lamellae during crystallization.[32-34] Nevertheless, in our case of the PCL/PEG blend, the diminishing of the amorphous layer thickness $l_a$ is much more evident than that for the crystalline thickness $l_c$ (Figure 4(c)). For this reason, we suggest that the decrease of long period observed in our case cannot be attributed solely to the rearrangement or thinning process of the crystal domains. Instead, the ongoing segregation of the PEG from PCL amorphous layer (allowing a better mobility of the PEG molecules) should be the major contribution to the decrease of the long period $L$ of the PCL lamellae during the competition between phase separation and crystallization.

In the late stage of crystallization (IV), the lamellae domain size and the crystalline structure are fully developed and stabilized, whereas the number of the lamellar domains, thus the crystallinity $X_c$ and the scattering invariant $Q$ of the system, continue to grow (Figure 4(b)). On the other hand, the PEG gradually segregating from the lamellar PCL domains can be trapped in the interfibril or interspherulite domains during the late stage of crystallization (images of Figure 2). We emphasize that the morphology of the PEG trapped in the final stage relates closely to the competition process between the liquid-liquid phase separation and the crystallization. And a control of the onset time for crystallization $t_{onset,WAXS}$ by the isothermal crystallization temperature $T_c$ provides a way to influence the competition process for a preferred morphology, as we have shown previously in preparing a tunable porous structure using the same system discussed here.[20] For instance, a lower isothermal crystallization temperature, thus an earlier $t_{onset,WAXS}$, leads to a smaller domains of PEG in the late stage.

## Conclusions

Combing SAXS/DSC and WAXS/DSC, we have traced the structural evolution of a PCL/PEG polymer blend, quenched below the melting temperature of PCL from a melting state. The structural evolution can be characterized by the four stages of the crystallization of PCL: the induction stage (I), the nucleation stage (II), the growth stage (III), and the late stage (IV). The characteristics observed in these four stages have been explained on the basis of the competition between the liquid-liquid phase separation and the crystallization of the system. An environment control favoring either LLPS or crystallization provides a possible method in preparing kinetically trapped morphologies for practical applications.

## References

(1) T. P. Russel and J. T. Koberstein, *J. Polym. Sci.*, **23**, 1109 (1985).
(2) W. Bras, G. E. Derbyshire, A. Devine, S. M. Clark, J. Cooker, B. E. Komanschek, and A. J. Ryan, *J. Appl. Cryst.*, **28**, 26 (1995).
(3) D. Lexa, *Rev. Sci. Instrum.*, **70**, 2242 (1999).
(4) K. N. Kruger and H. G. Zachmann, *Macromolecules*, **26**, 5202 (1993).
(5) S. Okamoto, K. Yamamoto, K. nomura, S. Hara, I. Akiba, K. Sakurai, A. Koyama, M. Nomura, and S. Sakurai, *J. Macromol. Sci. Phys.*, **43**, 279 (2004).
(6) C. Wutz, M. Bark, J. Cronauer, R. Dohrmann, and H. G. Zachmann, *Rev. Sci. Instrum.*, **66**, 1303 (1995).
(7) I. Sics, A. Nogales, T. A. Ezquerra, Z. Denchev, and F. J. Balta-Calleja, *Rev. Sci. Instrum.*, **71**, 1733 (2000).
(8) G. K. Bryant, H. F. Gleeson, A. J. Ryan, J. P. A. Fairclough, D. Bogg, J. G. P. Goossens, and W. Bras, *Rev. Sci. Instrum.*, **69**, 2114 (1998).

(9) S. Naylor, W. Bras, G. Derbyshire, G. R. Mant, D. Bogg, and A. J. Ryan, *Nucl. Instrum. Methods.*, **B97**, 253 (1995).
(10) N. J. Terrill, P. A. Fairclough, E. Towns-Ansrews, B. U. Komanschek, R. J. Young, and A. J. Ryan, *Polymer*, **39**, 2381 (1998).
(11) Lopez-Cabarcos, B. S. Hsiao, and F. J. Balta-Calleja, *Phys. Rev. E*, **54**, 989 (1996).
(12) K. Tashiro, S. Kariyo, A. Nishimori, T. Fujii, S. Saragai, S. Nakamoto, T. Kawaguchi, A. Matsumoto, and O. Rangsiman, *J. Polym. Sci.; Part B: Polym. Phys.*, **40**, 495 (2002).
(13) M. Imai, K. Kaji, and T. Kanaya, *Phys. Rev. Lett.*, **71**, 4162 (1993).
(14) P. D. Olmsted, W. C. K. Poon, T. C. B. McLeish, N. J. Terrill, and A. J. Ryan, *Phys. Rev. Lett.*, **81**, 373 (1998).
(15) H. Tanaka and T. Nishi, *Phys. Rev. Lett.*, **55**, 1102 (1985).
(16) N. Inaba, K. Sato, S. Suzuki, and T. Hashimoto, *Macromolecules*, **19**, 1690 (1986). N. Inaba, T. Yamada, S. Suzuki, and T. Hashimoto, *Macromolecules*, **21**, 407 (1988).
(17) J. K. Kim and B. K. Kim, *J. Polym. Sci.; Part B: Polym. Phys.*, **37**, 1991 (1999). J. K. Kim, B. K. Kim, and M. Park, *J. Polym. Sci.; Part B: Polym. Phys.*, **38**, 707 (2000).
(18) H. Wang, K. Shimizu, H. Kim, E. K. Hobbie, Z. Wang, and C. C. Han, *J. Chem. Phys.*, **116**, 7311 (2002).
(19) A. Keller and S. Z. D. Cheng, *Polymer*, **39**, 4461 (1998).
(20) W. T. Chuang, K. S. Shih, and P. D. Hong, *J. Polym. Res.*, **12**, 197 (2005).
(21) Y. H. Lai, Y. S. Sun, U. Jeng, Y. F. Song, K. L. Tsang, and K. S. Liang, *Nucl. Inst. Meth. Phys. Res. B*, **238**, 205 (2005).
(22) G. R. Strobl and M. Schneider, *J. Polym. Sci.; Part B: Polym. Phys.*, **18**, 1343 (1980).
(23) W. J. Ruland, *J. Appl. Crystallogr.*, **4**, 70 (1971).
(24) P. Debye and A. M. Bueche, *J. Appl. Phys.*, **20**, 518 (1949).
(25) P. Deby, H. R. Anderson, and H. Brumberger, *J. Appl. Phys.*, **28**, 679 (1957).
(26) R. S. Stein, F. B. Khambatta, F. P. Warner, T. P. Russell, A. Escala, and E. Balizer, *J. Polym. Sci., Polym. Symp.*, **3**, 313 (1978).
(27) T. P. Russell, H. Ito, and G. D. Wignall, *Macromolecules*, **21**, 1703 (1988).
(28) S. Nojima, K. Satoh, and T. Ashida, *Macromolecules*, **24**, 942 (1991).
(29) H. Hu and D. L. Dorset, *Macromolecules*, **23**, 4604 (1990).
(30) Z. G. Wang, B. S. Hsiao, E. B. Sirota, P. Agarwal, and S. Srinivas, *Macromolecules*, **33**, 978 (2000).
(31) G. Elsner, H. G. Zachmann, and J. R. Milch, *Makromol. Chem.*, **182**, 657 (1981).
(32) B. S. Hsiao, G. Kenn, Corwin H, D. Q. Wu, and B. Chu, *Polymer*, **34**, 3986 (1993).
(33) R. Verma, H. Maeand, and B. S. Hsiao, *Macromolecules*, **29**, 7767 (1996).
(34) H. Hama and K. Tashiro, *Polymer*, **44**, 2159 (2003).